



Research paper



Linearization of dynamic equations for vibration and modal analysis of flexible joint manipulators

Thanh-Trung Do, Viet-Hung Vu ^{*}, Zhaoheng Liu

Department of Mechanical Engineering, École de technologie supérieure, 1100 Notre-Dame St W, Montreal, H3C 1K3, Canada

ARTICLE INFO

Keywords:

Flexible robots
Lagrange dynamics
Linearization
Modal analysis

ABSTRACT

This paper presents the dynamic model and analytical modal analysis for robotic manipulators with rigid links and flexible joints. Dynamic equations of general robots with both prismatic and revolute joints are firstly developed using the Lagrangian formulation in minimal joint and motor coordinates. Next, linearized dynamic equations taking into account the influence of gravity forces, external forces, and control parameters are formulated based on the Taylor series. Therefore, the robot's modal parameters can be computed for any configuration based on a state-space matrix derived from the linearization model. To illustrate the proposed method, modal parameters of a flexible joint robot with six degrees of freedom are computed using the analytical method and estimated using the operational modal technique based on the vector autoregression model. Results obtained by both methods agree very well with each other.

1. Introduction

The dynamic behavior of mechanical systems, such as structures, machines, and robotic systems, is characterized by modal information, including three parameters: natural frequencies, damping ratios, and mode shapes. When available, these parameters can be used to predict the system's local dynamic behavior, set up a default detection and diagnostics baseline, or update the system's stiffness and damping parameters [1]. In machining operations, the knowledge about modal parameters in the workspace is very important because they can be used to adjust cutting parameters appropriately to improve machining accuracy, i.e., to avoid chatter vibration [2].

In practical applications, the estimation of modal parameters is complicated because it is necessary to conduct experiments to measure physical quantities at specific points using sensors, such as position, velocity, acceleration signals and even excitation forces/moments.

The well-known experimental modal analysis technique (EMA) [3] can be used to identify the modal parameters of mechanical systems. This technique requires output and input responses (excitation forces/momenta) for modal parameter estimation algorithms. The measured data is used to establish frequency response functions (FRFs) [4]. Therefore, modal parameters can be extracted from these functions. For the EMA technique, the excitation forces can be generated by impact hammers, and then both excitation forces and acceleration signals are measured simultaneously using force sensors and accelerometers.

In machining operations, the measurement of excitation forces of a machine for the modal analysis is complicated because excitation sources are affected by several factors, such as random loads and the controller of the machine. In addition, it is unfeasible to stop the working machine to measure input and output responses. The cost of force sensors is also an essential factor that should be taken into account. The use of output-only responses to identify modal parameters leads to an innovative technique called operational

* Corresponding author.

E-mail addresses: thanh-trung.do.1@ens.etsmtl.ca (T.-T. Do), viet-hung.vu@etsmtl.ca (V.-H. Vu), zhaoheng.liu@etsmtl.ca (Z. Liu).

modal analysis (OMA) [5]. For this technique, modal parameters can be extracted from output responses in the time/frequency domain.

The estimation of modal parameters for robotic systems is challenging because such systems are considered as time-varying systems. In [6,7], the author used the EMA technique to estimate modal parameters of industrial robots in their workspace. In [8], the vector autoregression model is used to identify modal information of the lightweight Scompi robot in working operations. The dynamic behavior of a milling robot depending on its configurations was investigated in [9] in which robot's modal parameters are extracted using the OMA technique based on the transmissibility function-based method (TFB) [10]. Overall, modal parameters of a robot depend on its configuration [11,12] in which the robot's parameters such as mass, inertia, stiffness, damping parameters are assumed to be constant. In several works such as [13–15], the authors have pointed out that the controller's effect should be considered for estimating modal parameters.

Most works mentioned above estimate modal parameters of a robot at several points in the robot's workspace. The main reason is that the use of the EMA technique, for example, to identify modal parameters, is costly and time-consuming. Generally, it is impossible to conduct modal tests at every robot's configuration in its workspace.

Recently, several authors have developed analytical methods to compute modal parameters of flexible multibody and robotic systems [16,17]. These methods have been developed based on linearized equations [18,19]. The most advantage of this approach is that modal parameters can be computed in the whole workspace. However, analytical methods require knowledge about the robot's kinematic/dynamic parameters.

A new analytical formulation is proposed to compute modal parameters of flexible-joint manipulators in which the influence of gravity forces, external forces and PD control parameters is taken into account. The robot's full modal mapping can be obtained in a single computation run when the kinematic/dynamic parameters are predetermined. This modal mapping is beneficial because it allows us to quickly extract the robot's modal information at the desired configuration. For the validation purpose, the OMA technique based on the vector autoregression (VAR) model is used to estimate modal parameters from motor positions instead of from acceleration signals as the traditional approach.

The rest of the paper is organized as follows. In Section 2, the dynamical model of flexible joint robots is presented using the Lagrangian formulation. Next, the PD controller with the gravity compensation is discussed in order to establish the closed-loop dynamics for analytical modal analysis. In Section 3, the state-space matrix is formulated to compute modal parameters. In Section 4, frequencies and damping ratios of a 6-DOF Scompi flexible joint robot with both prismatic/revolute joints are computed. The OMA technique based on the VAR model is used to re-estimated modal parameters obtained from the analytical model. Finally, conclusions are given in Section 5.

2. Dynamics of flexible-joint robots

2.1. Assumptions

In order to derive equations of motion of a general robot with n flexible joints, the following assumptions adapted from [20] are used in this work:

1. All links are considered as rigid bodies, in which the link $(i + 1)$ is controlled by the motor i fixed to the link i .
2. All flexible joints are considered as lumped-parameter models.
3. Gear ratios of the motors are large, (> 100).

By using the last assumption [21], equations of motion of the robot can be written in reduced form. Note that this form is benefit for the model-based control [22].

2.2. Dynamic equations

Based on the Lagrangian formulation [23], equations of motion of a general flexible-joint robot are expressed in a matrix form as follows:

$$\begin{bmatrix} \mathbf{M}(q) & \mathbf{0} \\ \mathbf{0} & \mathbf{B} \end{bmatrix} \begin{bmatrix} \ddot{\mathbf{q}} \\ \ddot{\mathbf{q}}_m \end{bmatrix} + \begin{bmatrix} \mathbf{C}(q, \dot{q})\dot{q} \\ \mathbf{0} \end{bmatrix} + \begin{bmatrix} \mathbf{g}(q) \\ \mathbf{0} \end{bmatrix} + \begin{bmatrix} \mathbf{D} & \mathbf{0} \\ \mathbf{0} & \mathbf{D}_m \end{bmatrix} \begin{bmatrix} \dot{\mathbf{q}} \\ \dot{\mathbf{q}}_m \end{bmatrix} + \begin{bmatrix} \mathbf{K}\mathbf{W}^2 & -\mathbf{K}\mathbf{W} \\ -\mathbf{K}\mathbf{W} & \mathbf{K} \end{bmatrix} \begin{bmatrix} q \\ q_m \end{bmatrix} = \begin{bmatrix} \mathbf{J}^T(q)\tau_{ext} \\ \tau_m \end{bmatrix} \quad (1)$$

in which all terms in Eq. (1) are explained in Appendix A.

In the literature [20,24,25], authors considered flexible-joint robots with revolute joints only. By using the matrix \mathbf{W} proposed in this work, dynamic equations of flexible-joint robots are derived in a general form in which both prismatic and revolute joints are considered.

2.3. Closed-loops dynamics

In order to study the dynamic behavior of a flexible joint robot, controllers should be used to track/follow the reference paths or points in the joint/task space. These controllers are used to solve two main control problems: tracking control and set-point control, in which the vector of motor torques τ_m is often formulated based on feedback signals measured using sensors implemented in the robot. In [20,26], several control strategies were proposed to compute τ_m , such as the simple PID control, the feedforward+PD control, and computed-torque control.

For the modal analysis problem of a flexible joint robot in its workspace, the simple PD control scheme with gravity compensation proposed in [27] is applied for the set-point control. This controller is the special case of the model-based feedforward+PD method [26]. Based on this control law, the desired (reference) position of joints is: $q^d = \text{const}$, while their velocity and acceleration are: $\dot{q}^d = \mathbf{0}$ and $\ddot{q}^d = \mathbf{0}$. Therefore, the motor torque vector is formulated as follows:

$$\tau_m = \underbrace{\mathbf{W}^{-1} (\mathbf{g}(q^d) - \mathbf{J}^T(q^d)\tau_{\text{ext}})}_{\text{feedforward}} + \underbrace{\mathbf{K}_P(q_m^d - q_m) - \mathbf{K}_D\dot{q}_m}_{\text{PD controller}} \quad (2)$$

where \mathbf{K}_P and \mathbf{K}_D are proportional and derivative gain matrices, respectively. These matrices can be chosen as diagonal positive definite matrices to guarantee the system stability. In Eq. (2), q_m^d is the desired position of motors (rotors) which is determined from the first line of Eq. (1) by setting $\dot{q}^d = \mathbf{0}$ and $\ddot{q}^d = \mathbf{0}$. Thus, one obtains:

$$q_m^d = \mathbf{W}q^d + (\mathbf{K}\mathbf{W})^{-1}(\mathbf{g}(q^d) - \mathbf{J}^T(q^d)\tau_{\text{ext}}) \quad (3)$$

Substituting Eq. (2) into Eq. (1) leads to $2n$ closed-loop dynamic equations as follows:

$$\Gamma \triangleq \begin{bmatrix} \mathbf{M}(q)\ddot{q} + \mathbf{C}(q, \dot{q})\dot{q} + \mathbf{g}(q) + \mathbf{D}\dot{q} + \mathbf{K}\mathbf{W}(\mathbf{W}q - q_m) - \mathbf{J}^T(q)\tau_{\text{ext}} \\ \mathbf{B}\dot{q}_m + \mathbf{D}_m\ddot{q}_m - \mathbf{K}(\mathbf{W}q - q_m) - \mathbf{W}^{-1}(\mathbf{g}(q^d) - \mathbf{J}^T(q^d)\tau_{\text{ext}}) - \mathbf{K}_P(q_m^d - q_m) + \mathbf{K}_D\dot{q}_m \end{bmatrix} = \mathbf{0} \quad (4)$$

3. Analytical modal analysis

3.1. Linearization

By using the following definitions:

$$\mathbf{z} \triangleq [\mathbf{q}^T, q_m^T]^T, \dot{\mathbf{z}} \triangleq [\dot{\mathbf{q}}^T, \dot{q}_m^T]^T, \text{ and } \ddot{\mathbf{z}} \triangleq [\ddot{\mathbf{q}}^T, \ddot{q}_m^T]^T \quad (5)$$

Eq. (4) can be rewritten in a compact form as:

$$\Gamma(\ddot{\mathbf{z}}, \dot{\mathbf{z}}, \mathbf{z}) = \mathbf{0} \quad (6)$$

The linearized dynamic equations of a flexible joint robot can be derived using the Taylor series expansion [18,19] about an ‘equilibrium position’ $\{\ddot{\mathbf{z}}^d, \dot{\mathbf{z}}^d, \mathbf{z}^d\}$ defined by:

$$\ddot{\mathbf{z}}^d = \begin{bmatrix} \mathbf{0} \\ \mathbf{0} \end{bmatrix}, \quad \dot{\mathbf{z}}^d = \begin{bmatrix} \mathbf{0} \\ \mathbf{0} \end{bmatrix}, \quad \mathbf{z}^d = \begin{bmatrix} \mathbf{q}^d \\ q_m^d \end{bmatrix} \quad (7)$$

Consequently, the linearized equations can be expressed as follows:

$$\overline{\mathbf{M}}\Delta\ddot{\mathbf{z}} + \overline{\mathbf{D}}\Delta\dot{\mathbf{z}} + \overline{\mathbf{K}}\Delta\mathbf{z} = \mathbf{0} \quad (8)$$

where $\Delta\ddot{\mathbf{z}} = \ddot{\mathbf{z}} - \ddot{\mathbf{z}}^d$, $\Delta\dot{\mathbf{z}} = \dot{\mathbf{z}} - \dot{\mathbf{z}}^d$ and $\Delta\mathbf{z} = \mathbf{z} - \mathbf{z}^d$ represent the perturbation vectors about the desired equilibrium position $\{\ddot{\mathbf{z}}^d, \dot{\mathbf{z}}^d, \mathbf{z}^d\}$. In addition, three matrices $(\overline{\mathbf{M}}, \overline{\mathbf{D}}$, and $\overline{\mathbf{K}} \in \mathbb{R}^{2n \times 2n}$) in Eq. (8) are determined by:

$$\overline{\mathbf{M}} \triangleq \frac{\partial \Gamma}{\partial \ddot{\mathbf{z}}} \Big|_{(\ddot{\mathbf{z}}^d, \dot{\mathbf{z}}^d, \mathbf{z}^d)} = \begin{bmatrix} \mathbf{M}(q^d) & \mathbf{0} \\ \mathbf{0} & \mathbf{B} \end{bmatrix}, \quad (9)$$

$$\overline{\mathbf{D}} \triangleq \frac{\partial \Gamma}{\partial \dot{\mathbf{z}}} \Big|_{(\ddot{\mathbf{z}}^d, \dot{\mathbf{z}}^d, \mathbf{z}^d)} = \begin{bmatrix} \mathbf{D} & \mathbf{0} \\ \mathbf{0} & \mathbf{D}_m + \mathbf{K}_D \end{bmatrix}, \quad (10)$$

$$\overline{\mathbf{K}} \triangleq \frac{\partial \Gamma}{\partial \mathbf{z}} \Big|_{(\ddot{\mathbf{z}}^d, \dot{\mathbf{z}}^d, \mathbf{z}^d)} = \begin{bmatrix} \mathbf{K}_G(q^d) + \mathbf{K}\mathbf{W}^2 & -\mathbf{K}\mathbf{W} \\ -\mathbf{K}\mathbf{W} & \mathbf{K} + \mathbf{K}_P \end{bmatrix} \quad (11)$$

where the matrix $\mathbf{K}_G \in \mathbb{R}^{n \times n}$ is derived as follows:

$$\mathbf{K}_G(q^d) = \left. \frac{\partial \mathbf{g}(q)}{\partial q} \right|_{q^d} - \left. \frac{\partial (\mathbf{J}^T(q)\tau_{\text{ext}})}{\partial q} \right|_{q^d} \quad (12)$$

It can be seen that two matrices $\overline{\mathbf{M}}$ and $\overline{\mathbf{K}}$ depend on the robot’s configuration, i.e., the vector of joint coordinates q^d . Furthermore, the matrices $\overline{\mathbf{D}}$ and $\overline{\mathbf{K}}$ are functions of damping and stiffness coefficients at joints/motors, as well as the stiffness and damping gains of the controller. The effect of the gravity forces and external forces/moment on the stiffness system is also included in Eq. (12) that makes more/less ‘artificial stiffness’ into the stiffness matrix $\overline{\mathbf{K}}$. Note that the effect of the controller on the modal parameters was also discussed in [28] for linear systems, in which the positive position feedback (PPF) control used to modify dynamic behavior of linear systems is similar to the PD control law presented above.

To the best of our knowledge, the linearized model of a general robot with both flexible revolute/prismatic joints presented in Eq. (8) including the effects of gravity and external forces/moment Eq. (12) is firstly proposed in this study.

3.2. Modal parameters in the workspace

By assuming that the physical robot's parameters (masses, positions of center of masses, inertia tensor, and stiffness/damping parameters), as well as the gain matrices \mathbf{K}_P and \mathbf{K}_D of the PD controller are constants and predetermined, Eq. (8) can be used for the analytical modal analysis (AMA) of the robot. Because the damping matrix \mathbf{D} is non-proportional, modal parameters can be found by solving the following eigenvalue problem [28]:

$$(\mathbf{A} - \lambda_k \mathbf{I}) \mathbf{y}_k = \mathbf{0} \quad (13)$$

where the state matrix $\mathbf{A} \in \mathbb{R}^{4n \times 4n}$ is derived from the linearized mass, damping and stiffness matrices, $(\bar{\mathbf{M}}, \bar{\mathbf{D}}$ and $\bar{\mathbf{K}})$ as follows:

$$\mathbf{A} = \begin{bmatrix} \mathbf{0} & \mathbf{I} \\ -\bar{\mathbf{M}}^{-1} \bar{\mathbf{K}} & -\bar{\mathbf{M}}^{-1} \bar{\mathbf{D}} \end{bmatrix} \quad (14)$$

where \mathbf{I} denotes the identity matrix. If a eigenvalue λ_k is found from the characteristic polynomial, $\det(\mathbf{A} - \lambda_k \mathbf{I}) = 0$, a corresponding eigenvector $\mathbf{y}_k \in \mathbb{C}^{4n}$ can be therefore obtained from Eq. (13). In practice, λ_k may be real and/or a pair of complex conjugate numbers. Therefore, three different cases may occur [29]:

- Case 1: If all eigenvalues have negative real parts, i.e., lie on the left-hand side of the complex plane, then the dynamic behavior of the robot at q^d is asymptotically stable.
- Case 2: If at least one of eigenvalues has a positive real part, i.e., lies on the right-hand side of the complex plane, then the dynamic behavior of the robot at q^d is unstable. Therefore, gain matrices need to be changed appropriately to achieve stability.
- Case 3: If one of eigenvalues has zero real part, then dynamic behavior of the robot at q^d may be stable or unstable.

For the under-damped case, all eigenvalues are complex numbers. A complex conjugate pair can be expressed as:

$$\lambda_{k,k^*} = -\omega_k \zeta_k \pm j \omega_k \sqrt{1 - \zeta_k^2} \quad (15)$$

for $k = 1, \dots, 2n$. As a result, a natural frequency ω_k and a damping ratio ζ_k are computed from λ_k as follows:

$$\omega_k = \sqrt{\text{real}(\lambda_k)^2 + \text{imag}(\lambda_k)^2} \quad (\text{rad/s}), \quad (16)$$

$$\zeta_k = -\frac{\text{real}(\lambda_k)}{\omega_k} \quad (17)$$

where $f_k = \frac{\omega_k}{2\pi}$ (Hz). In addition, a complex mode shape vector $\mathbf{u}_k \in \mathbb{C}^{2n}$ corresponding to ω_k and ζ_k is determined from the first $2n$ elements of the eigenvector \mathbf{y}_k [28]:

$$\mathbf{u}_k = [\mathbf{I} \quad \mathbf{0}] \mathbf{y}_k \quad (18)$$

As a result, modal parameters of a flexible joint robot (for given the desired positions of joint coordinates q^d , all kinematic/dynamic parameters and the PD controller gains) are computed using the following steps:

- Step 1: Evaluate the mass matrix $\mathbf{M}(q^d)$ and the matrix $\mathbf{K}_G(q^d)$ using Eq. (12).
- Step 2: Compute the linearized mass, damping and stiffness matrices using Eqs. (9)–(11).
- Step 3: Establish the state matrix using Eq. (14).
- Step 4: Solve eigenvalue problem using Eq. (13) in order to find eigenvalues λ_k and eigenvectors \mathbf{y}_k for $k = 1, \dots, 2n$.
- Step 5: Extract natural frequencies, damping ratios and mode shapes using Eqs. (16)–(18).

Note that in the 'Step 4', the `eig` function in Matlab can be used to solve the eigenvalue problem using the numerical method.

4. Numerical simulation

4.1. Scompi robot and its parameters

The lightweight Scompi robot with six degrees of freedom developed at Hydro Quebec research institute is shown in Fig. 1. The robot is designed to be quickly installed on a track and to perform in the confined space for machining tasks of large complex hydro-power equipment such as grinding, polishing and welding [30].

The Scompi robot has a total weight about 39 (kg) including six rigid links connected together by six joints, in which the first joint is a prismatic joint, and the others are revolute joints. All joints are driven by stepping motors coupled to harmonic drivers with high gear ratios. The first joint is designed based on the rack-and-pinion mechanism in which r_1 is the rack gear's radius [30] defined by $r_1 = 0.057(\text{m})$ [31]. For other revolute joints, $r_i = 1$, for $i = 2, \dots, 6$. In addition, the stiffness and damping parameters of the Scompi robot [32] are presented in Table 1.

For the kinematic modeling of the Scompi robot, the standard Denavit–Hartenberg (DH) convention is used [33,34] in which the DH parameters are listed in Table 2.

The other dynamic parameters including masses, inertia tensors, positions of the center of masses, gear ratios obtained from manufacturers or CAD data are presented in Tables 3 and 4.

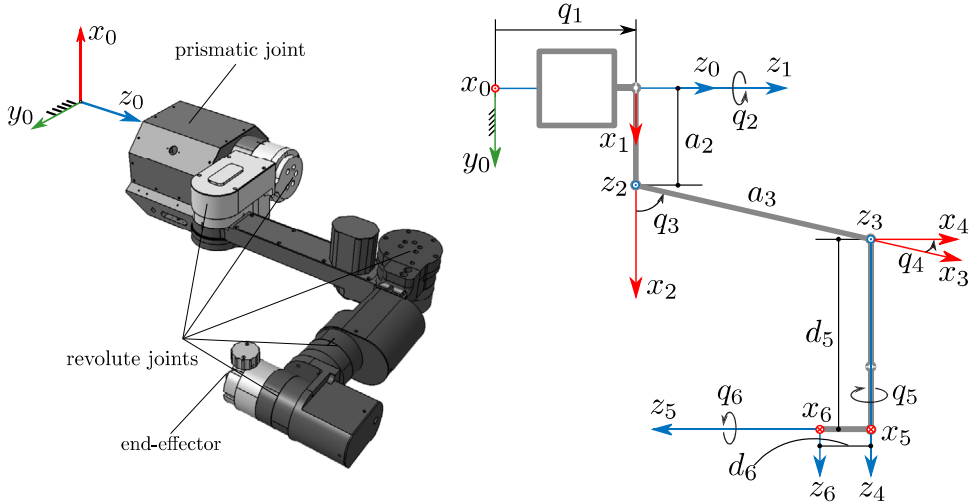


Fig. 1. Model of the Scompi robot (left) and its kinematic representation using the standard Denavit–Hartenberg convention (right).

Table 1

Damping/stiffness parameters of joints and motors.

i	1	2	3	4	5	6	Scale factor	Unit
$d_{f,i}$	2.73	24.74	5.76	9.37	8.74	8.74	1	(N s/m) or (N m s/rad)
$d_{fm,i}$	9.46	9.46	9.46	9.46	5.90	5.90	10^{-4}	(N m s/rad)
k_i	25	120	120	57	29	29	1000	(N m/rad)

Table 2

DH parameters of the Scompi robot with $a_2 = 0.192$, $a_3 = 0.420$, $d_5 = 0.380$, and $d_6 = 0.088$.

Link	1	2	3	4	5	6	Unit
θ_i	$\frac{\pi}{2}$	q_2	q_3	q_4	q_5	q_6	(rad)
d_i	q_1	0	0	0	d_5	d_6	(m)
a_i	0	a_2	a_3	0	0	0	(m)
α_i	0	$\frac{\pi}{2}$	0	$\frac{\pi}{2}$	$\frac{\pi}{2}$	$-\frac{\pi}{2}$	(rad)

Table 3

Physical parameters of rigid links.

	Link 1	Link 2	Link 3	Link 4	Link 5	Link 6	Unit
m_i	19.0000	5.7230	5.1660	4.4250	3.3020	1.0220	(kg)
$x_{C,i}$	0.0210	-0.0540	-0.1380	0.0110	0.0	-0.0040	(m)
$y_{C,i}$	0.0310	0.0030	0.0	0.0120	-0.0260	0.0390	(m)
$z_{C,i}$	-0.2260	0.0140	-0.0190	0.1610	-0.0220	0.0	(m)
$I_{xx,i}$	0.0	0.0100	0.0080	0.0440	0.0120	0.0010	(kg m ²)
$I_{xy,i}$	0.0	0.0030	0.0	0.0	0.0	0.0	(kg m ²)
$I_{xz,i}$	0.0	-0.0030	-0.0100	0.0020	0.0	0.0	(kg m ²)
$I_{yz,i}$	0.0	0.0440	0.1600	0.0440	0.0060	0.0010	(kg m ²)
$I_{zy,i}$	0.0	0.0	0.0	0.0070	-0.0010	0.0	(kg m ²)
$I_{zz,i}$	0.0	0.0430	0.1600	0.0080	0.0080	0.0120	(kg m ²)

Table 4

Gear ratios and inertia moments of motors.

i	1	2	3	4	5	6	Scale factor	Unit
N_i	51	160	160	160	160	160	1	(-)
$I_{t_i,z}$	1.71	2.65	2.42	1.26	0.91	0.86	10^{-4}	(kg m ²)

4.2. Simulation results

Using the analytical formulation presented in Section 3, modal parameters of the Scompi robot are computed in two cases:

Case 1: There is no robot's tool.

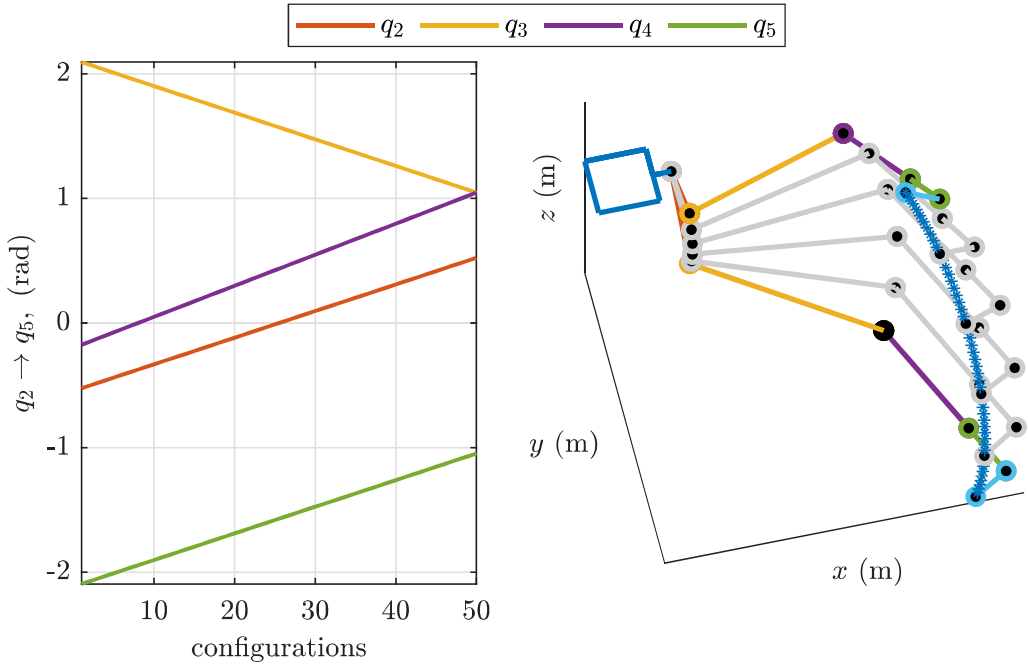


Fig. 2. Different configurations of the robot in its workspace for computing modal parameters: robot's joints depending on configurations (left), robot' configurations in the Cartesian space (right).

Case 2: A tool with the mass $m_E = 4$ (kg) is added to the end-effector.

To illustrate modal parameters of the Scompi robot in its workspace, 50 joint's configurations shown in Fig. 2 are used in which several configurations are plotted for illustration purpose. The first and last joints are hold constant with $q_1^d = 0$ (m) and $q_6^d = 0$ (rad), and other joints are varied linearly in the following intervals:

$$q_2^d \in [-\frac{\pi}{6}, \frac{\pi}{6}], q_3^d \in [\frac{2\pi}{3}, \frac{\pi}{3}], q_4^d \in [-\frac{\pi}{18}, \frac{\pi}{3}], q_5^d \in [-\frac{2\pi}{3}, -\frac{\pi}{3}]$$

For simplification, external forces/moment are set to zero, $\tau_{ext} = 0$. In addition, the inertia tensor and position of the center of mass for the robot's tool are set to zero, i.e., $I_E^{(n)} = 0$ and $s_E^{(n)} = 0$ with $n = 6$.

In addition, the gain matrices K_p and K_d in Eqs. (9) and (10) for both cases are:

$$K_p = 1000 \text{ diag}(15, 15, 15, 15, 15, 15) \quad (19)$$

$$K_d = \text{diag}(52, 52, 52, 52, 52, 52) \quad (20)$$

Modal parameters of twelve modes are computed simultaneously using Matlab 2018b, in which the computation time for one configuration is approximately 0.003(s) using a Laptop with 12 Gb memory, Intel Core i7, CPU @2.20 GHz. The simulation results for 50 configurations are shown in Figs. 3 and 4.

It can be seen in Fig. 3 that the lowest frequency is about 5.13 (Hz), while the highest frequency is 851.14 (Hz). Because the robot's tool is added to the end-effector, the natural frequency curves for the first case are clearly lower than those for the second case. In addition, the frequencies for modes 8, 9, 10, and mode 11 change significantly when adding the extra mass to the end-effector in which the deviations are approximately 12.08 (Hz), 11.70 11.60 (Hz), and 49 (Hz). In modes 4, 5, 6, and mode 12, their frequencies are nearly constant, i.e., they are independent to the robot's configuration. The modes 4 and 5 are closely spaced modes [35] because their frequencies are close the common mean, approximately 12.88 (Hz).

On the other hand, the damping ratios presented in Fig. 4 vary in the range: from 1.25 (%) for mode 7 to 80.61 (%) for mode 12. In practice, modes with high damping ratios are often ignored or are difficult to observe because the system does not vibrate or vibrate in a very short time. Generally, the damping ratio curves for the first case are lower than those for the second case except for mode 7. Most damping ratios for all modes are less than 27 (%). In the last mode, the damping ratios are greater than 80 (%) for both cases. It can be seen that damping ratios in modes 4 and 5 in two cases are nearly constant, approximately 16.16 and 16.71 (%). Besides, modes 4, 5 and 12 are nearly independent of the robot's configuration.

Obviously, natural frequencies and damping ratios of the Scompi robot change very complicated in its workspace, and they depend clearly on the robot's configurations. Therefore, the linearized model proposed is advantageous in achieving the configuration-dependent modal parameters for flexible joint robots.

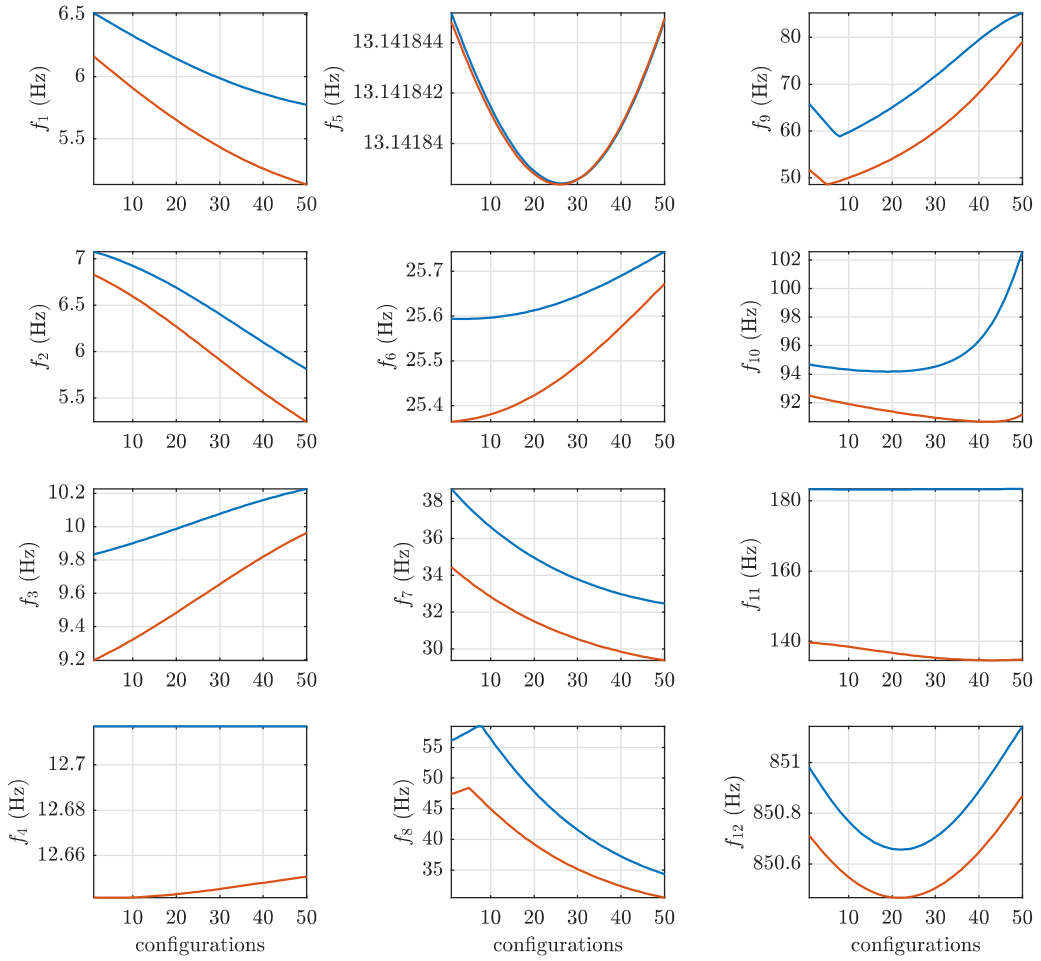


Fig. 3. Undamped natural frequencies for 50 configurations: without additional mass (blue line), with additional mass (orange line). (For interpretation of the references to color in this figure legend, the reader is referred to the web version of this article.)

Furthermore, the influence of controller gains on natural frequencies and damping ratios of the first and second modes (case 1) is shown in Fig. 5. For numerical simulations, diagonal elements of the matrix \mathbf{K}_P are set to be equal and changed linearly from 2000 to 15 000, $K_D = 0.425\sqrt{K_P}$, and other parameters are hold constant. For example, at the first configuration, the first frequency rises from 2.39 to 6.51 (Hz), the first damping ratio declines from 9.44 to 7.85 (%). For these modes, when increasing diagonal elements of \mathbf{K}_P , natural frequencies of the Scompi robot increase, while its damping ratios decrease.

The effect of flexible coefficient on the first and second mode shapes (case 1) is shown in Fig. 6 with two values of controller gains $K_{P,ii} = 12\,000$ and $15\,000$ ($i = 1, \dots, 6$). Because eigenvalues obtained from Eq. (18) are complex vectors, they are therefore presented in polar coordinates in which one component of an eigenvector is described by a phase and a logarithmic magnitude. Note that in Fig. 6, the first six components of eigenvectors corresponding to modal coordinates of six joints are plotted.

4.3. Validation

To validate the Scompi's modal parameters obtained using the analytical model presented in Section 4.2, the OMA technique based on the VAR method in the time domain is applied [8,36]. One the most advantage of the OMA technique is that modal parameters can be extracted from output-only response, such as position, velocity and acceleration signals. The input responses (excitation forces/momenta) do not need to measure because they are considered as white noise processes [5].

In order to produce the output responses, an impulse force is applied at the end-effector along y_0 -axis with the amplitude 50 (N) in the time interval $t \in [0.2, 0.2 + 6\Delta t]$ (s) with $\Delta t = 0.001$ (s). The PD controller with gravity compensation described by Eq. (2) is used to compute the motor torques for vibration reduction under the external force (see Figs. B.1 and B.2 in Appendix B). Therefore, the output responses can be obtained by solving the direct dynamics problem described in Eq. (1) using numerical integration methods, e.g., ode-solvers in Matlab.

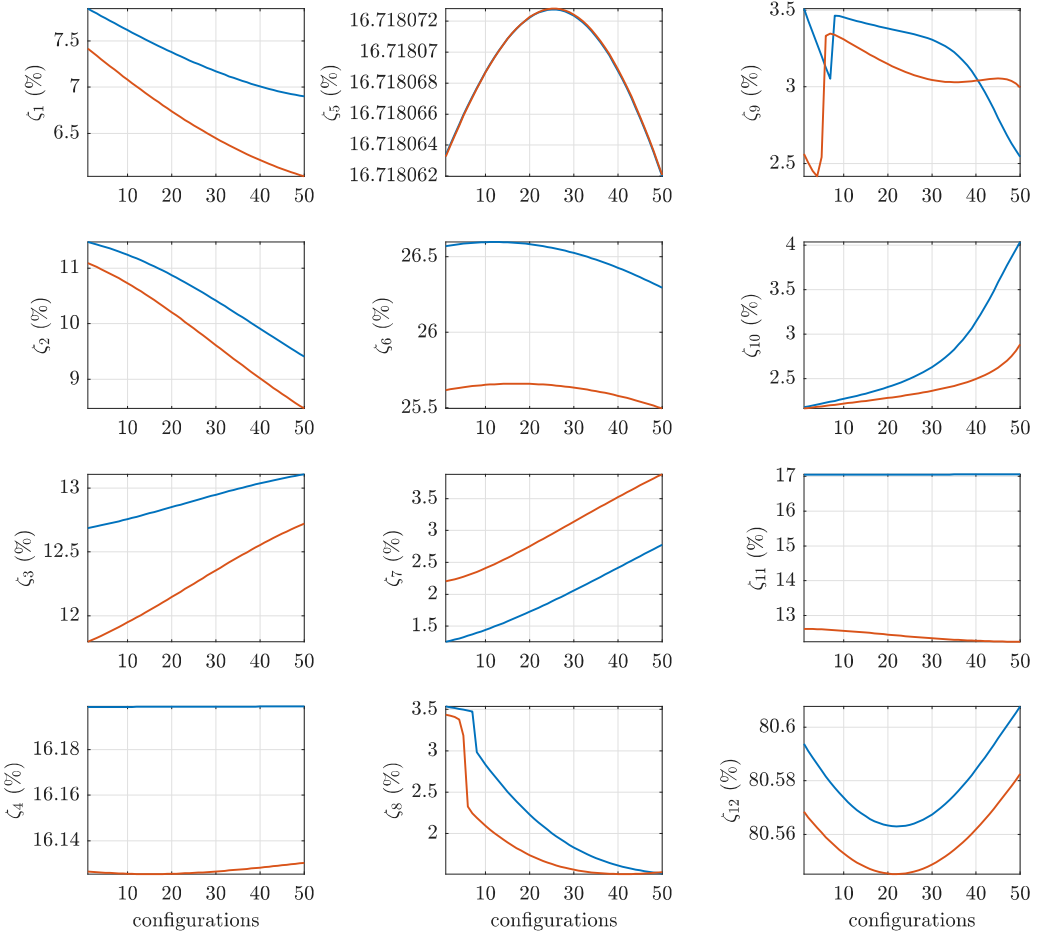


Fig. 4. Damping ratios for 50 configurations: without additional mass (blue line), with additional mass (orange line). (For interpretation of the references to color in this figure legend, the reader is referred to the web version of this article.)

For the direct dynamics, an initial condition of joint coordinates at $t = 0$ (s) can be selected from 50 configurations presented in Fig. 2. For example, if the 8th configuration is chosen as an initial condition, then we have:

$$\mathbf{q}(0) = [0.0, -0.374, 1.9448, 0.0, -1.9448, 0.0]^T \quad (21)$$

while the initial condition of motor coordinates is computed from Eq. (3) with zero external forces/momenta:

$$\mathbf{q}_m(0) = [0.0, -0.374, 1.9446, -0.0001, -1.9449, 0.0]^T \quad (22)$$

At $t = 0$ (s), we assume that $\dot{\mathbf{q}}(0) = \dot{\mathbf{q}}_m(0) = \mathbf{0}$.

Using the function `ode45` in Matlab with the fixed step integration $\Delta t = 0.001$ (s), motor positions (angles) in the degree with respect to time are shown in Fig. 7. It can be seen that motor positions are reduced exponentially to the desired values for a short time using the feedforward+PD controller. From motor positions (output responses), the Scompi robot's modal parameters can be identified using the VAR method. Note that motor positions are used to identify modal parameters because they can be measured very accurately using encoders integrated into all motor drivers.

To estimate modal parameters, a very high model order range, the order from 2 to 100, is investigated. For each model order, matrices of autoregressive parameters (ARs) are firstly computed using pseudo-inverse method based on QR or SVD techniques. Next, a discrete state-space matrix for eigenvalue problem is derived from ARs [37]. Therefore, modal parameters including undamped natural frequencies, damping ratios and complex mode shapes can be extracted from eigenvalues and eigenvectors of the discrete state-space matrix. For example, stabilization diagrams describing all frequencies and damping ratios versus the model orders are illustrated in Fig. 8 (case 1) and Fig. 9 (case 2). In addition, the information about complex mode shapes is used to eliminate unstable frequencies/damping ratios using single-mode validation criteria proposed in [35] such as the relative eigenfrequency and damping ratio differences, modal assurance criterion (MAC), as well as the order modal assurance (OMAC) [37].

To identify physical modes, i.e., modes appearing in complex conjugate pairs, the grid algorithm implemented in the NAFID-tool is applied [38]. The main idea of this algorithm is to automatically search frequencies/damping ratios with small deviations in the

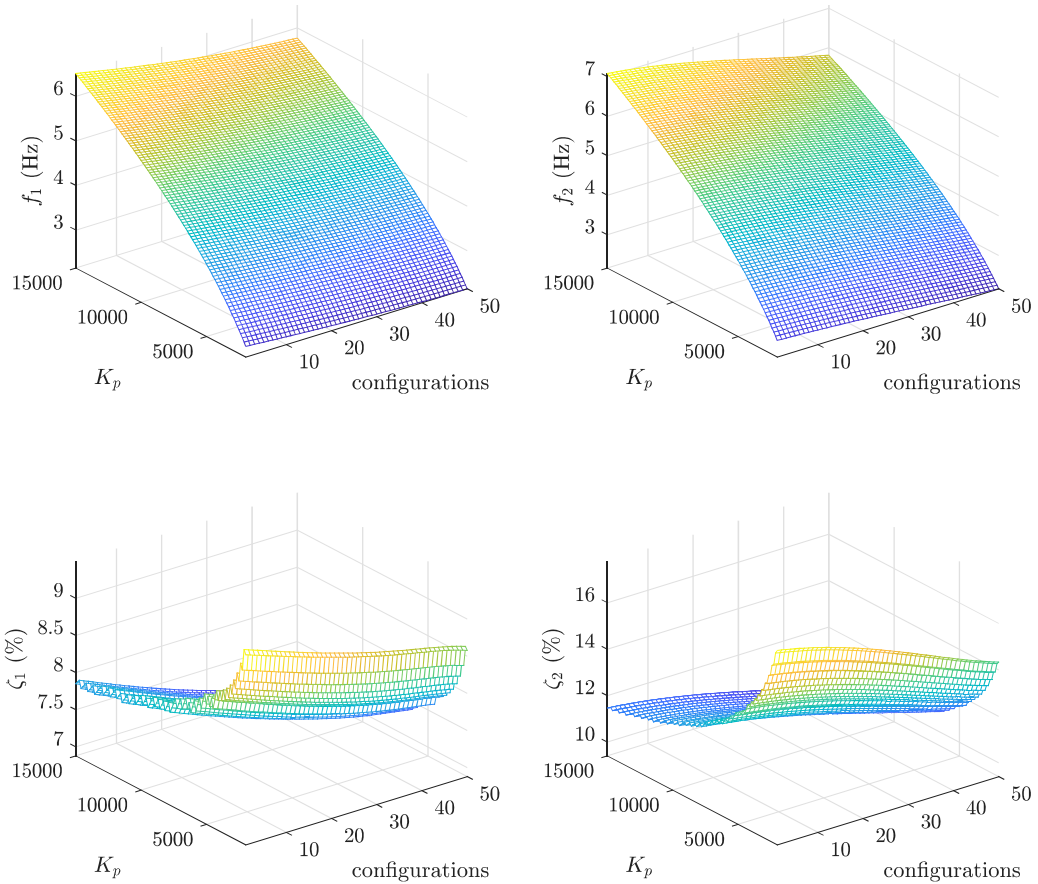


Fig. 5. Frequencies and damping ratios depending on controller gains.

Table 5

Frequencies and damping ratios corresponding to the 8th configuration obtained using AMA and OMA methods.

Mode	AMA-Case 1		OMA-Case 1		AMA-Case 2		OMA-Case 2	
	f (Hz)	ζ (%)						
1	6.3692	7.6686	6.4191	7.6685	5.9634	7.1538	6.0133	7.1538
2	6.9642	11.2981	6.9191	11.3001	6.6522	10.8175	6.6133	10.8185
3	9.8842	12.7399	9.9191	12.7214	9.2928	11.9109	9.3133	11.8997
4	12.7170	16.1988	12.7170	16.2361	12.6414	16.1256	12.6133	16.1264
5	13.1418	16.7181	13.1191	16.7334	13.1418	16.7181	13.1133	16.7640
6	25.5949	26.5926	25.6191	26.6241	25.3752	25.6469	25.4133	25.6637
7	37.0199	1.3938	37.0197	1.4237	33.1574	2.3513	33.1133	2.3514
8	58.3984	2.9817	58.4191	3.0212	46.3479	2.1881	46.3133	2.1703
9	58.8631	3.4643	58.8191	3.4564	49.3412	3.3381	49.3133	3.3375
10	94.3825	2.2483	94.4191	2.2508	92.0281	2.2052	92.0275	2.1623
11	183.2303	17.0471	183.2191	17.0463	138.7911	12.5831	138.8000	12.5469
12	850.8082	80.5774	-	-	850.5782	80.5557	-	-

given ranges (frequency/damping resolutions) along the model-order axis. If the number of frequencies/damping values found is equal or greater than the number of repeating frequencies defined by the user, then frequencies/damping ratios in these ranges are considered to be stable. In NAFID-tool, the default values of frequency and damping resolutions are 0.1 (Hz) and 0.1 (%), respectively. For example, the red points marked by green squares in Fig. 9 represent stable vibration modes because their undamped frequencies and damping ratios are nearly constant along the model-order axis. The blue points are unstable frequencies/damping ratios due to computational error or noise.

The natural frequencies and damping ratios obtained using the analytical and VAR methods are summarized in Table 5. There are eleven stable frequencies/damping ratios identified using the NAFID-tool in which the computation time is approximately 120 (s). It can be seen that the results obtained show an excellent matching. However, the 12th mode is very difficult to identify, even

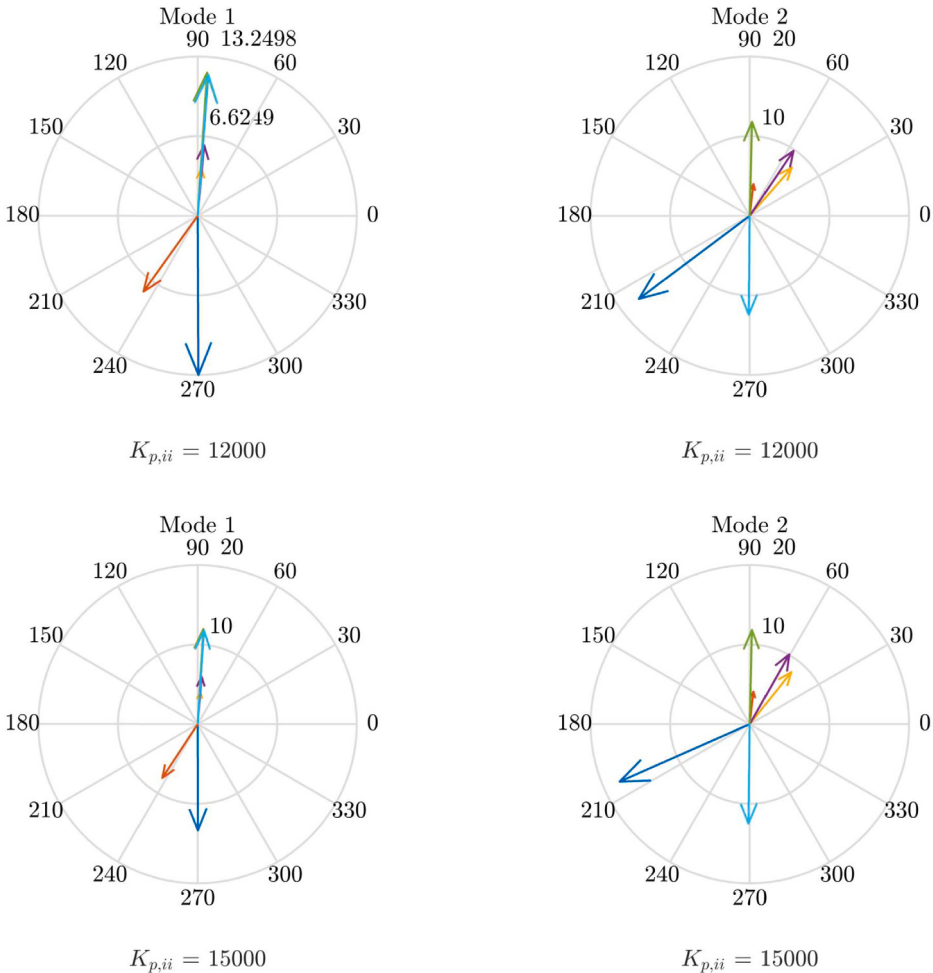


Fig. 6. Complex mode shapes depending on controller gains.

the fixed time step Δt is set to 0.0005 (s) to detect the highest frequency (the Nyquist frequency) up to 1000 (Hz). It can explain by the fact that the last mode has a very high damping ratio, > 80 (%) for both two cases.

Furthermore, acceleration signals of the end-effectors are also used to estimate modal parameters (see Fig. B.2 in Appendix B). However, there are eight stable modes found using NAFID-tool (see Fig. B.3). It can be inferred that the motor position signals may contain more ‘useful information’ for the modal parameter estimation than that obtained from the end-effector’s acceleration signals. This exploration may be considered a promising aspect of future research.

Overall, numerical simulations prove that the proposed formulation for the modal analysis can be used to compute natural frequencies and damping ratios of flexible-joint robots in the workspace.

5. Conclusions

Analytical formulations for the dynamic simulation and computing modal parameters of flexible-joint robots in their workspace are presented in this paper. First, dynamic equations of a general robot with prismatic and revolute joints are established based on the Lagrangian formulation, and then linearized equations for the modal analysis are derived using the Taylor series expansion. Using the proposed formulations, natural frequencies and damping ratios depend on the robot’s configuration, the gravity and external forces, and the control parameters. Modal parameters of the lightweight Scompi robot with six flexible joints are computed for various configurations. The results obtained from the analytical method are validated using the operational modal analysis technique based on the vector autoregression model in which the output responses for the identification problem are motor position signals instead of acceleration signals as traditional approaches. The proposed formulations can be used to identify stiffness and damping parameters of flexible joints and to optimize control parameters for vibration suppression. Future works include the effect of cutting forces and other control strategies on computing modal parameters.

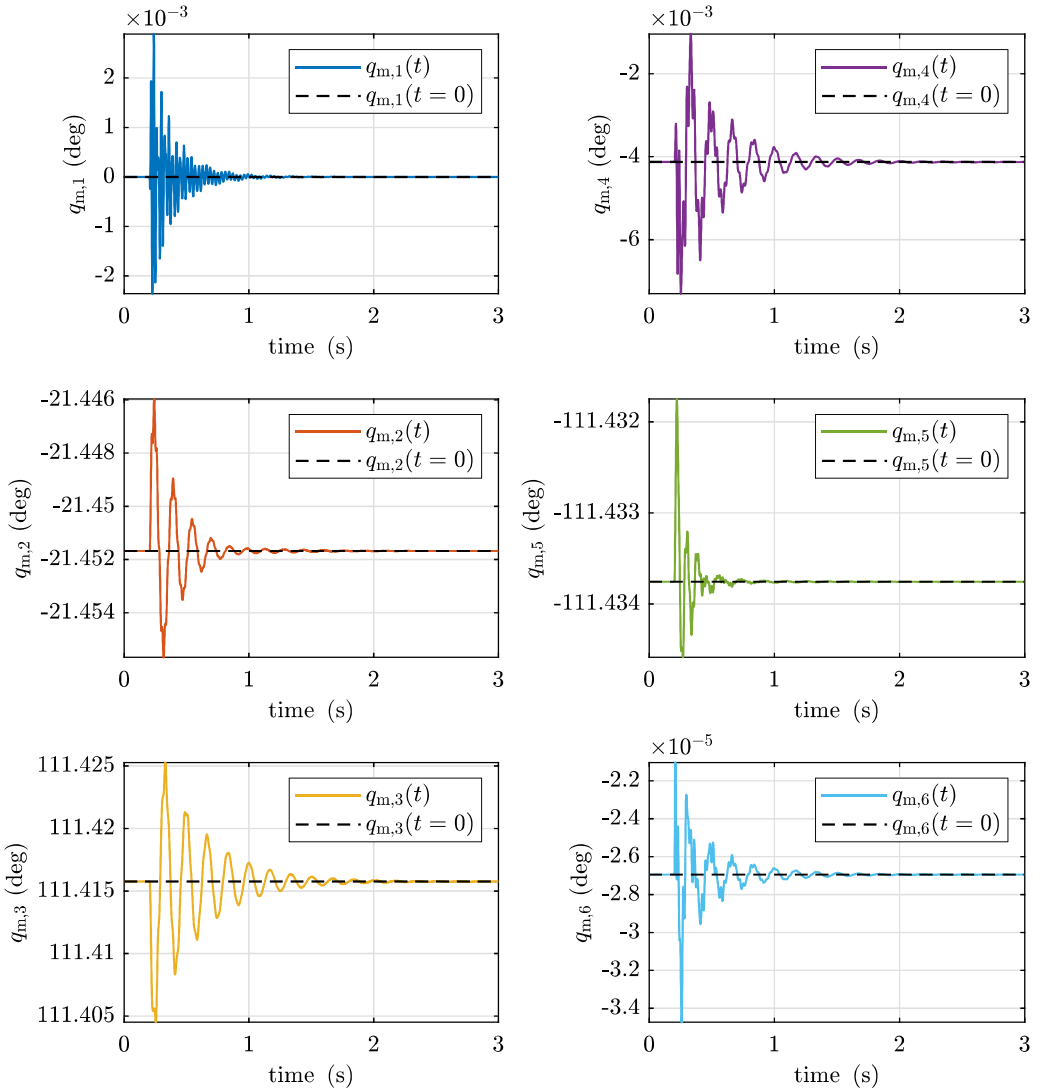


Fig. 7. Motor positions (case 2).

Declaration of competing interest

The authors declare that they have no known competing financial interests or personal relationships that could have appeared to influence the work reported in this paper.

Acknowledgment

The authors would like to acknowledge the financial support of the Natural Sciences and Engineering Research Council of Canada (NSERC), the grant numbers RGPIN-2016-05859 and RGPIN-2019-05749.

Appendix A

In this section, equations of motion of a general flexible-joint robot with prismatic and revolute joints are formulated. The effect of a robot's tool is also included in dynamic equations. All kinematic/dynamic parameters of the robot are assumed to be predetermined. Minimal coordinates of the robot include: a vector of joint coordinates $q = [q_1, q_2, \dots, q_n]^T$ and a vector of motor coordinates after reduction $q_m = [q_{m,1}, q_{m,2}, \dots, q_{m,n}]^T$.

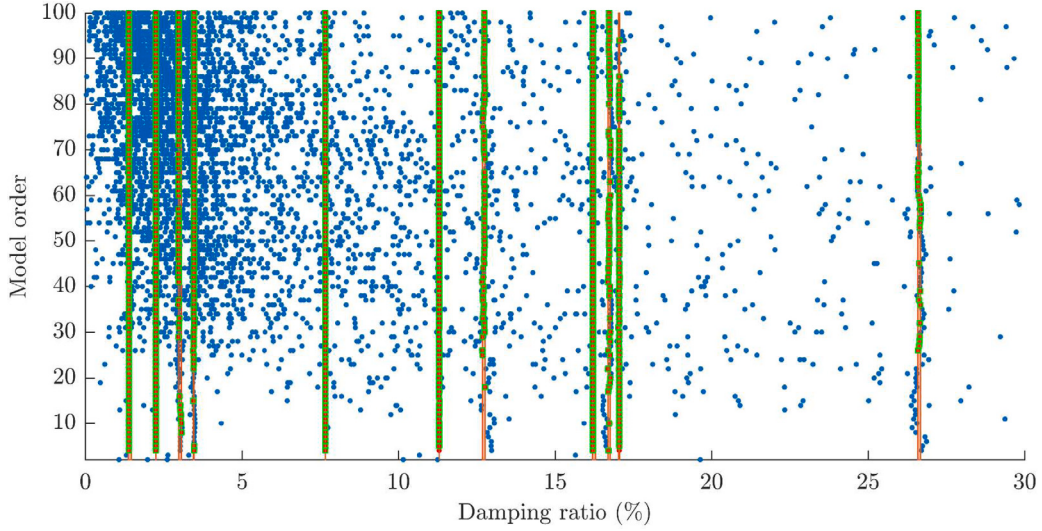
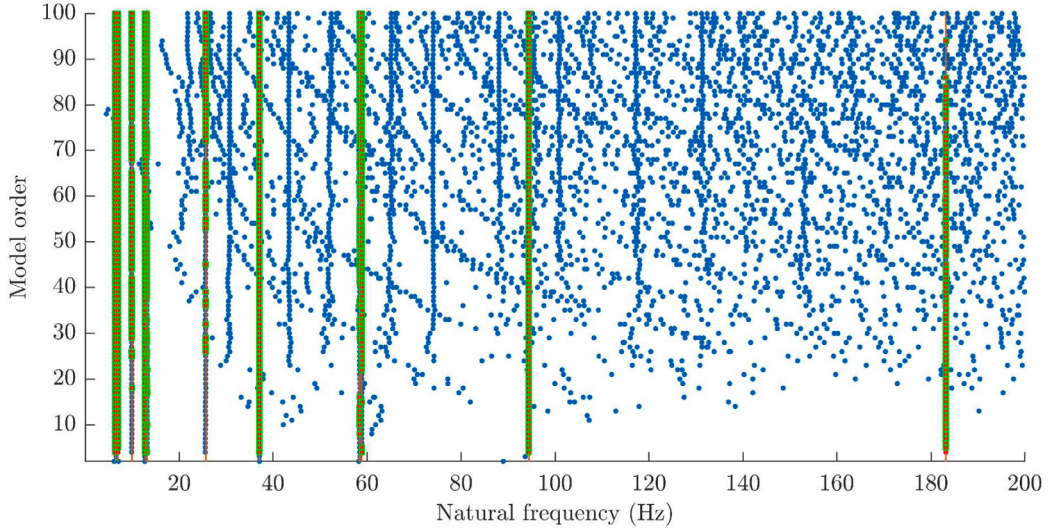


Fig. 8. Stable natural frequencies and damping ratios (green color) are identified from the motor positions (case 1). (For interpretation of the references to color in this figure legend, the reader is referred to the web version of this article.)

Using the standard Denavit–Hartenberg convention [33,34], the relative position and orientation of BF_i (body-fixed frame i at the origin O_i) with respect to BF_{i-1} (body-fixed frame $i-1$ at the origin O_{i-1}) are determined by a transformation matrix $T_i^{(i-1)} \in \mathbb{R}^{4 \times 4}$:

$$T_i^{(i-1)} = \begin{bmatrix} R_i^{(i-1)} & p_i^{(i-1)} \\ \mathbf{0} & 1 \end{bmatrix} \quad (\text{A.1})$$

where $p_i^{(i-1)} \in \mathbb{R}^3$ and $R_i^{(i-1)} \in \mathbb{R}^{3 \times 3}$ represent the position of O_i and orientation of BF_i , respectively. Therefore, the absolute position and orientation of the link i in IF_0 (the inertial reference frame), are derived as:

$$T_i^{(0)} = T_1^{(0)} T_2^{(1)} \dots T_{i-1}^{(i-2)} T_i^{(i-1)} = \begin{bmatrix} R_i^{(0)} & p_i^{(0)} \\ \mathbf{0} & 1 \end{bmatrix} \quad (\text{A.2})$$

When $i = n$, $T_n^{(0)}$ represents the position and orientation of the last link.

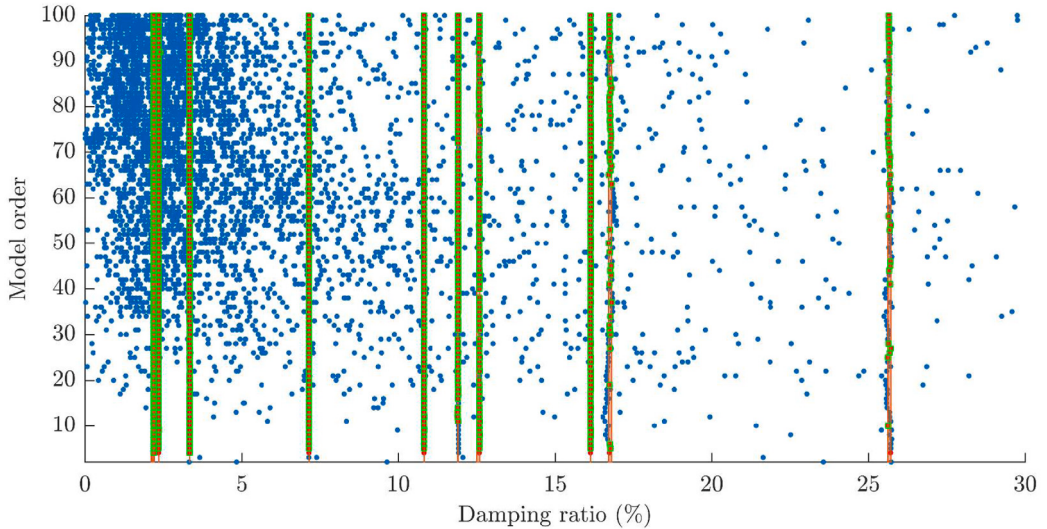
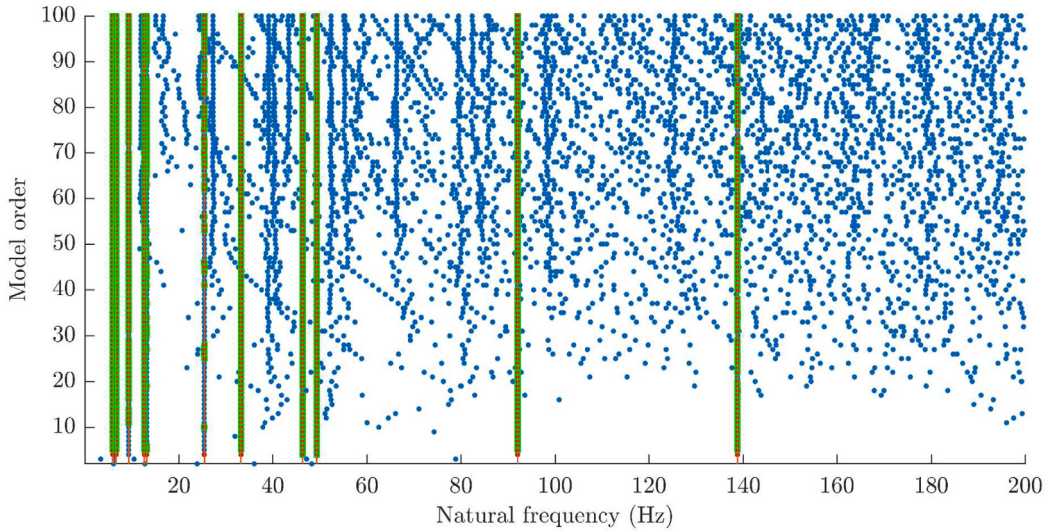


Fig. 9. Stable natural frequencies and damping ratios (green color) are identified from the motor positions (case 2). (For interpretation of the references to color in this figure legend, the reader is referred to the web version of this article.)

If C_i and E are the center of mass of the link i and robot's tool, then their absolute positions in IF_0 are computed using Eq. (A.2) as follows:

$$\mathbf{p}_{C_i}^{(0)} = \mathbf{p}_i^{(0)} + \mathbf{R}_i^{(0)} \mathbf{s}_i^{(i)} \quad (\text{A.3})$$

$$\mathbf{p}_E^{(0)} = \mathbf{p}_n^{(0)} + \mathbf{R}_n^{(0)} \mathbf{s}_E^{(n)} \quad (\text{A.4})$$

where $\mathbf{s}_i^{(i)}$ and $\mathbf{s}_E^{(n)} \in \mathbb{R}^3$ are the constant position vector of C_i and E in BF_i and BF_n , respectively. To take time derivative of Eqs. (A.3) and (A.4), one obtains $\dot{\mathbf{p}}_{C_i}^{(0)}$ and $\dot{\mathbf{p}}_E^{(0)}$.

The angular velocity matrix of link i in BF_i is defined by [23]:

$$\hat{\boldsymbol{\omega}}_i^{(i)} = (\mathbf{R}_i^{(0)})^\top (\dot{\mathbf{R}}_i^{(0)}) = \begin{bmatrix} 0 & -\omega_{i,z}^{(i)} & \omega_{i,y}^{(i)} \\ \omega_{i,z}^{(i)} & 0 & -\omega_{i,x}^{(i)} \\ -\omega_{i,y}^{(i)} & \omega_{i,x}^{(i)} & 0 \end{bmatrix} \quad (\text{A.5})$$

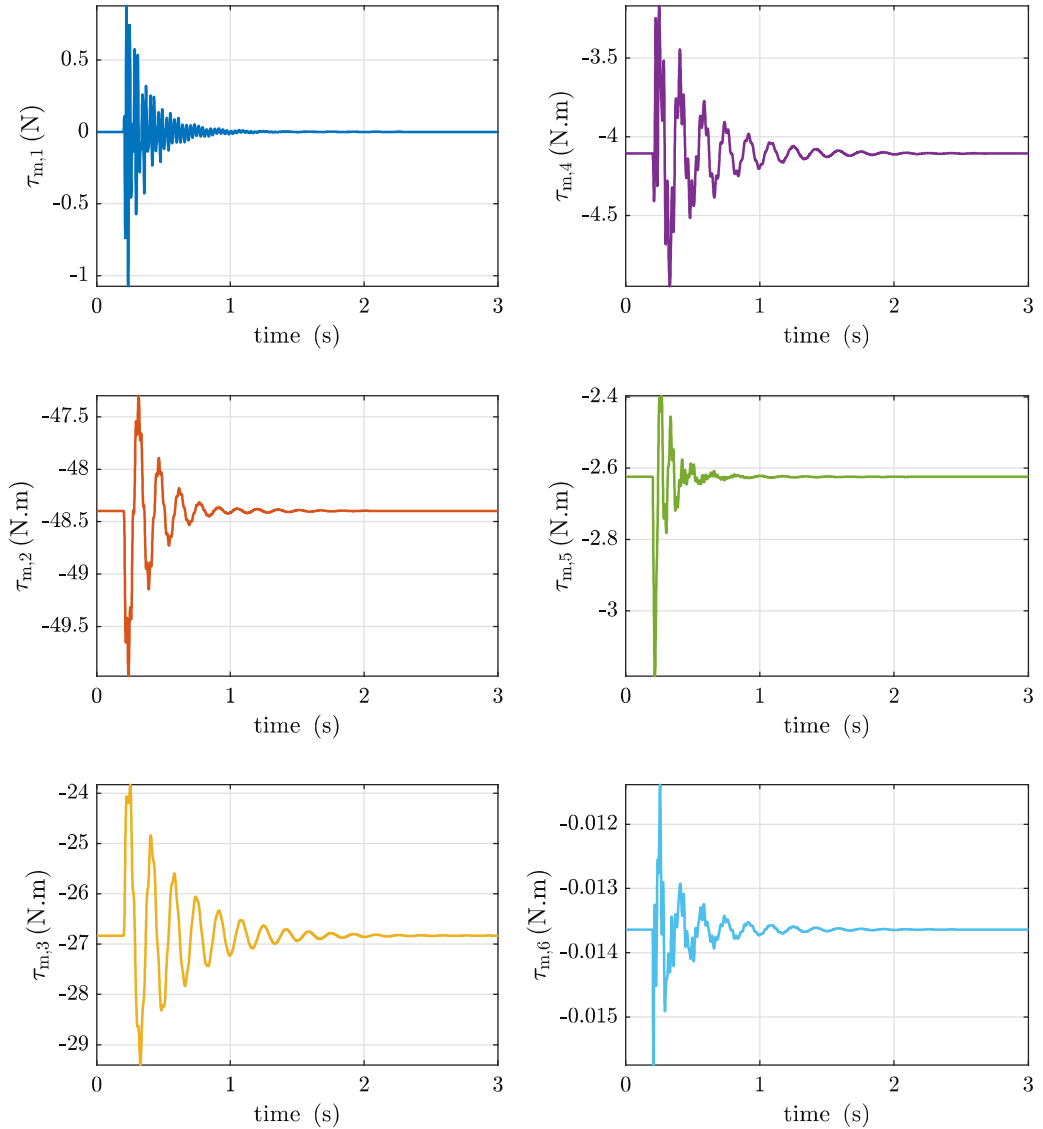


Fig. B.1. Motor torques (case 2).

and its angular velocity vector in BF_i is:

$$\boldsymbol{\omega}_i^{(i)} = \begin{bmatrix} \omega_{i,x}^{(i)} & \omega_{i,y}^{(i)} & \omega_{i,z}^{(i)} \end{bmatrix}^T \quad (\text{A.6})$$

The angular velocity matrix of the robot's tool in IF_0 is computed as [23]:

$$\hat{\boldsymbol{\omega}}_E^{(0)} = (\dot{\boldsymbol{R}}_n^{(0)})(\boldsymbol{R}_n^{(0)})^T = \begin{bmatrix} 0 & -\omega_{n,z}^{(0)} & \omega_{n,y}^{(0)} \\ \omega_{n,z}^{(0)} & 0 & -\omega_{n,x}^{(0)} \\ -\omega_{n,y}^{(0)} & \omega_{n,x}^{(0)} & 0 \end{bmatrix} \quad (\text{A.7})$$

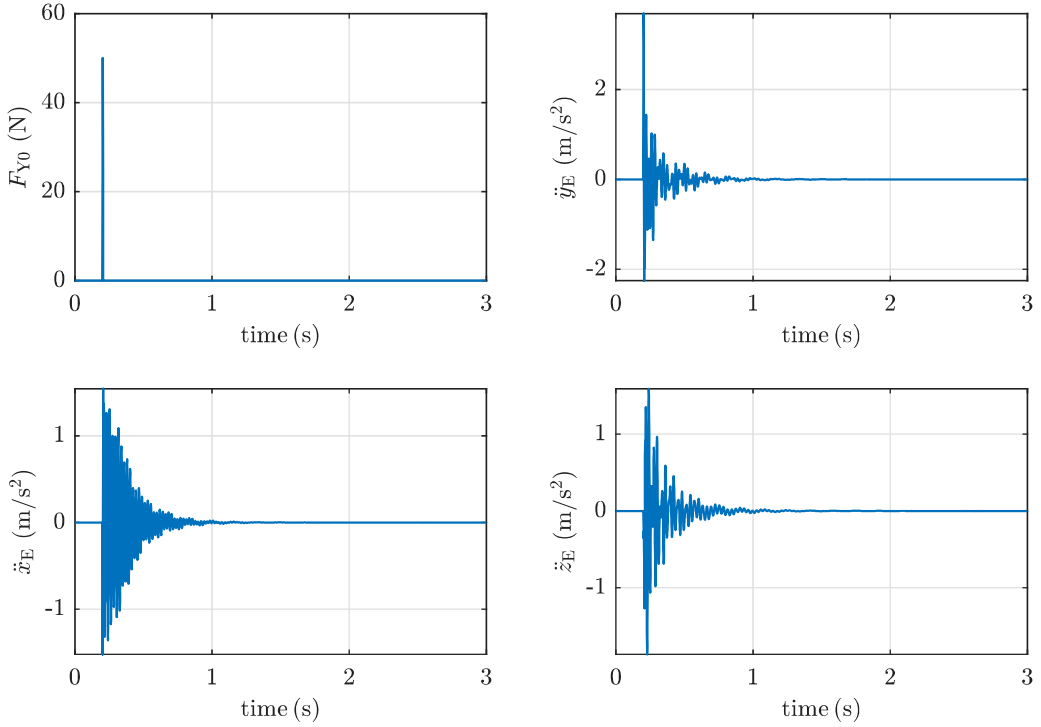


Fig. B.2. Impact force and linear accelerations of the end-effector (case 2).

and its angular velocity vector in IF_0 is:

$$\boldsymbol{\omega}_E^{(0)} = \begin{bmatrix} \omega_{n,x}^{(0)} & \omega_{n,y}^{(i)} & \omega_{n,z}^{(0)} \end{bmatrix}^T \quad (\text{A.8})$$

Using the assumptions mentioned in Section 2.1, the angular velocity vector of the rotor i in RF_i (rotor-fixed frame i) is reduced to [20]:

$$\boldsymbol{\omega}_{r_i}^{(r_i)} = \mathbf{R}_{i-1}^{(r_i)} \boldsymbol{\omega}_{i-1}^{(i-1)} + [0 \ 0 \ N_i \dot{q}_{m,i}]^T \approx [0 \ 0 \ N_i \dot{q}_{m,i}]^T \quad (\text{A.9})$$

where $\mathbf{R}_{i-1}^{(r_i)}$ is the constant rotation matrix of BF_{i-1} with respect to RF_i , N_i (> 100) and $\dot{q}_{m,i}$ is the gear ratio and coordinate of the motor i , respectively. The linear velocity of the rotor's center of mass does not need to be computed because the mass of motor i is combined into the mass of link $i-1$.

The torsional deflection e_i of flexible joint i is defined as follows:

$$e_i = \begin{cases} q_i - q_{m,i} & \text{if the joint } i \text{ is revolute} \\ \frac{q_i}{r_i} - q_{m,i} & \text{if the joint } i \text{ is prismatic} \end{cases} \quad (\text{A.10})$$

where r_i represents the ‘characteristic radius’ of the joint’s driver i which is used to convert the rotational motion of the motor i to the translational motion of the joint i .

The kinetic energy of all links, the robot’s tool and rotors is computed as follows:

$$\begin{aligned} K = & \frac{1}{2} \sum_{i=1}^n \left(m_i (\dot{\mathbf{p}}_{C_i}^{(0)})^T \dot{\mathbf{p}}_{C_i}^{(0)} + (\boldsymbol{\omega}_i^{(i)})^T \mathbf{I}_i^{(i)} \boldsymbol{\omega}_i^{(i)} \right) + \\ & \frac{1}{2} m_E (\dot{\mathbf{p}}_E^{(0)})^T \dot{\mathbf{p}}_E^{(0)} + \frac{1}{2} (\boldsymbol{\omega}_E^{(0)})^T \mathbf{I}_E^{(0)} \boldsymbol{\omega}_E^{(0)} + \frac{1}{2} \sum_{i=1}^n (\boldsymbol{\omega}_{r_i}^{(r_i)})^T \mathbf{I}_{r_i}^{(r_i)} \boldsymbol{\omega}_{r_i}^{(r_i)} \\ = & \frac{1}{2} \dot{\mathbf{q}}^T \mathbf{M} \dot{\mathbf{q}} + \frac{1}{2} \dot{\mathbf{q}}_m^T \mathbf{B} \dot{\mathbf{q}}_m \end{aligned} \quad (\text{A.11})$$

where m_i and $\mathbf{I}_i^{(i)} \in \mathbb{R}^{3 \times 3}$ are the mass and inertia tensor of the link i about C_i in BF_i ; m_E and $\mathbf{I}_E^{(0)}$ is the mass and inertia tensor of the robot’s tool about E in IF_0 ; $\mathbf{I}_{r_i}^{(r_i)} \in \mathbb{R}^{3 \times 3}$ is the inertia tensor of rotor i in RF_i ; $\mathbf{M} \in \mathbb{R}^{n \times n}$ are the mass matrix of the robot’s links and tool. The matrix \mathbf{B} is defined by:

$$\mathbf{B} = \text{diag}(N_1^2 \mathbf{I}_{r_1,z}, N_2^2 \mathbf{I}_{r_2,z}, \dots, N_n^2 \mathbf{I}_{r_n,z}) \quad (\text{A.12})$$

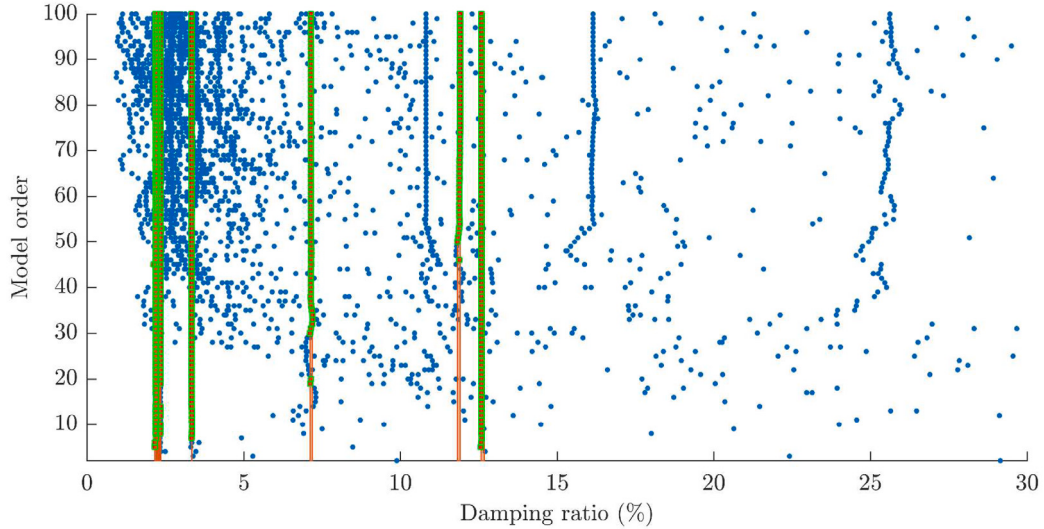
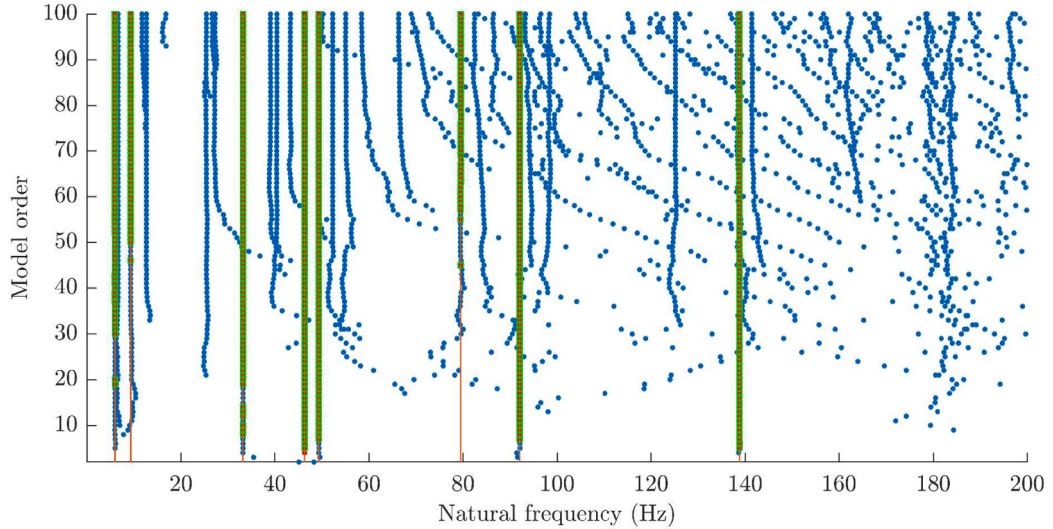


Fig. B.3. Stable natural frequencies and damping ratios (green color) are identified from the end-effector accelerations (case 2). (For interpretation of the references to color in this figure legend, the reader is referred to the web version of this article.)

where $I_{r_i,z}$ is the inertial moment of the rotor i about its rotating z -axis.

The potential energy is computed as follows:

$$\begin{aligned} P &= \frac{1}{2} \sum_{i=1}^n k_i e_i^2 - \sum_{i=1}^n m_i g_0^T p_{C_i}^{(0)} - m_E g_0^T p_E^{(0)} \\ &= \frac{1}{2} (\mathbf{W} q - q_m)^T \mathbf{K} (\mathbf{W} q - q_m) - \sum_{i=1}^n m_i g_0^T p_{C_i}^{(0)} - m_E g_0^T p_E^{(0)} \end{aligned} \quad (\text{A.13})$$

where k_i the stiffness coefficient of the motor shaft i ; $g_0 \in \mathbb{R}^3$ is the gravity vector in IF_0 . Here, the matrices \mathbf{W} and \mathbf{K} are defined by:

$$\mathbf{W} = \text{diag}\left(\frac{1}{r_1}, \frac{1}{r_2}, \dots, \frac{1}{r_n}\right) \quad (\text{A.14})$$

$$\mathbf{K} = \text{diag}(k_1, k_2, \dots, k_n), \quad (\text{A.15})$$

Note that $r_i = 1$ if the joint i is revolute, $i = (1, \dots, n)$.

The Rayleigh dissipation function is computed as follows:

$$\Phi = \frac{1}{2} \sum_{i=1}^n d_{f,i} \dot{q}_i^2 + \frac{1}{2} \sum_{i=1}^n d_{fm,i} \dot{q}_{m,i}^2 = \frac{1}{2} \dot{q}^T D \dot{q} + \frac{1}{2} \dot{q}_m^T D_m \dot{q}_m \quad (\text{A.16})$$

where $d_{f,i}$ and $d_{fm,i}$ are viscous coefficients of joint i on the link side and on the motor side, respectively.

$$D = \text{diag}(d_{f,1}, d_{f,2}, \dots, d_{f,n}), \quad (\text{A.17})$$

$$D_m = \text{diag}(d_{fm,1}, d_{fm,2}, \dots, d_{fm,n}) \quad (\text{A.18})$$

The virtual work of nonconservative forces is computed as follows:

$$\delta W = (J^T \tau_{\text{ext}}^{(0)})^T \delta q + \tau_m^T \delta q_m \quad (\text{A.19})$$

where $\tau_{\text{ext}}^{(0)} \in \mathbb{R}^6$ is the vector of external forces and moments applied at E in IF₀; $J \in \mathbb{R}^{6 \times n}$ is the geometric Jacobian matrix [23] derived from $\dot{p}_E^{(0)}$ and $\omega_E^{(0)}$; $\tau_m \in \mathbb{R}^n$ is the vector of motor torques; δq and δq_m are vectors of virtual displacements.

From all kinematic/dynamic quantities presented above, equations of motion of the flexible-joint robot with n links and the robot's tool using the Lagrangian formulation [23] are expressed as follows:

$$M(q)\ddot{q} + C(q, \dot{q})\dot{q} + g(q) + D\dot{q} + KW(Wq - q_m) = J^T(q)\tau_{\text{ext}} \quad (\text{A.20})$$

$$B\ddot{q}_m + D_m\dot{q}_m - K(Wq - q_m) = \tau_m \quad (\text{A.21})$$

where $C \in \mathbb{R}^{n \times n}$ is the matrix of centrifugal/Coriolis terms and $g \in \mathbb{R}^n$ is the vector of gravity terms.

Appendix B

This section presents simulation results of the Scompi robot presented in Section 4.3 in which the mass $m_E = 4$ (kg) is added to the end-effector.

The motor torques are computed using the control law presented in Eq. (2) and the results obtained are shown in Fig. B.1. In addition, the linear accelerations of the end-effector \ddot{x}_E are derived from Eq. (A.4) in which \ddot{x}_E depends on joint variables, such as q , \dot{q} and \ddot{q} . Based on Eq. (1), these variables are computed using numerical integration methods. The simulation results of \ddot{x}_E are plotted in Fig. B.2. Using NAFID-tool, eight stable poles are identified as shown in Fig. B.3.

References

- [1] M.I. Friswell, J.E. Mottershead, *Finite Element Model Updating in Structural Dynamics*, Kluwer Academic Publishers, 1995.
- [2] G. Quintana, J. Ciurana, Chatter in machining processes: A review, Int. J. Mach. Tools Manuf. 51 (5) (2011) 363–376, <http://dx.doi.org/10.1016/j.ijmachtools.2011.01.001>.
- [3] N.M.M. Maia, J.M.M. Silva (Eds.), *Theoretical and Experimental Modal Analysis*, Research Studies Press, 1997.
- [4] D.J. Ewins, *Modal Testing: Theory, Practical and Applications*, second ed., Research Studies Press, 2000.
- [5] R. Brincker, C. Ventura, Introduction to Operational Modal Analysis, Wiley, 2015, <http://dx.doi.org/10.1002/9781118535141>.
- [6] A. Karim, J. Hitzer, A. Lechner, A. Verl, Analysis of the dynamic behavior of a six-axis industrial robot within the entire workspace in respect of machining tasks, in: 2017 IEEE International Conference on Advanced Intelligent Mechatronics (AIM), 2017, pp. 670–675, <http://dx.doi.org/10.1109/aim.2017.8014094>.
- [7] D. Hao, W. Wang, Z. Liu, C. Yun, Experimental study of stability prediction for high-speed robotic milling of aluminum, J. Vib. Control 26 (7–8) (2020) 387–398, <http://dx.doi.org/10.1177/1077546319880376>.
- [8] V.-H. Vu, Z. Liu, M. Thomas, W. Li, B. Hazel, Output-only identification of modal shape coupling in a flexible robot by vector autoregressive modeling, Mech. Mach. Theory 97 (2016) 141–154, <http://dx.doi.org/10.1016/j.mechmachtheory.2015.11.005>.
- [9] A. Maamar, V. Gagnol, T.-P. Le, L. Sabourin, Pose-dependent modal behavior of a milling robot in service, Int. J. Adv. Manuf. Technol. 107 (1) (2020) 527–533, <http://dx.doi.org/10.1007/s00170-020-04974-y>.
- [10] C. Devriendt, P. Guillaume, Identification of modal parameters from transmissibility measurements, J. Sound Vib. 314 (1) (2008) 343–356, <http://dx.doi.org/10.1016/j.jsv.2007.12.022>.
- [11] I. Zaghbani, V. Songmene, I. Bonev, An experimental study on the vibration response of a robotic machining system, J. Eng. Manuf. 227 (6) (2013) 866–880, <http://dx.doi.org/10.1177/0954405413477067>.
- [12] S. Mejri, V. Gagnol, T.-P. Le, L. Sabourin, P. Ray, P. Paultre, Dynamic characterization of machining robot and stability analysis, Int. J. Adv. Manuf. Technol. 82 (1) (2016) 351–359, <http://dx.doi.org/10.1007/s00170-015-7336-3>.
- [13] W. Bernzen, Active vibration control of flexible robots using virtual spring-damper systems, J. Intell. Robot. Syst. 24 (1999) 69–88, <http://dx.doi.org/10.1023/A:1008035116904>.
- [14] M. Chu, Y. Zhang, G. Chen, H. Sun, Effects of joint controller on analytical modal analysis of rotational flexible manipulator, Chin. J. Mech. Eng. 3 (28) (2015) 460–469, <http://dx.doi.org/10.3901/CJM.2015.0121.017>.
- [15] T.F.C. Berninger, S. Fuderer, D.J. Rixen, Modal analysis of a 7 dof sweet pepper harvesting robot, in: M.L. Mains, B.J. Dilworth (Eds.), *Topics in Modal Analysis and Testing*, Springer International Publishing, 2020, pp. 163–170.
- [16] I. Palomba, R. Vidoni, Flexible-link multibody system eigenvalue analysis parameterized with respect to rigid-body motion, Appl. Sci. 9 (23) (2019) <http://dx.doi.org/10.3390/app9235156>.
- [17] M. Bottin, S. Cocuzza, N. Comand, A. Doria, Modeling and identification of an industrial robot with a selective modal approach, Appl. Sci. 10 (13) (2020) <http://dx.doi.org/10.3390/app10134619>.
- [18] J.H. Ginsberg, *Advanced Engineering Dynamics*, second ed., Cambridge University Press, 1998.
- [19] A.G. Lynch, M.J. Vanderplough, A symbolic formulation for linearization of multibody equations of motion, J. Mech. Des. 117 (3) (1995) 441–445.
- [20] A. De Luca, W. Book, Robots with flexible elements, in: B. Siciliano, O. Khatib (Eds.), *Springer Handbook of Robotics*, second ed., Springer, 2016, pp. 243–282, http://dx.doi.org/10.1007/978-3-319-32552-1_11.

- [21] M.W. Spong, Modeling and control of elastic joint robots, *J. Dyn. Syst. Meas. Control* 109 (4) (1987) 310–318.
- [22] G. Buondonno, A. De Luca, A recursive Newton-Euler algorithm for robots with elastic joints and its application to control, in: 2015 IEEE/RSJ International Conference on Intelligent Robots and Systems (IROS), 2015, pp. 5526–5532, <http://dx.doi.org/10.1109/IROS.2015.7354160>.
- [23] B. Siciliano, L. Sciavicco, L. Villani, G. Oriolo, *Robotics Modelling, Planning and Control*, Springer, 2009.
- [24] A. De Luca, P. Tomei, Elastic joints, in: C. Canudas de Wit, B. Siciliano, G. Bastin (Eds.), *Theory of Robot Control*, Springer-Verlag, 1996, pp. 179–217.
- [25] C. Ott, *Cartesian Impedance Control of Redundant and Flexible-Joint Robots*, in: *Springer Tracts in Advanced Robotics*, Springer-Verlag, 2008.
- [26] A. De Luca, Feedforward/feedback laws for the control of flexible robots, in: IEEE International Conference on Robotics and Automation (ICRA), 2000, pp. 233–240, <http://dx.doi.org/10.1109/ROBOT.2000.844064>.
- [27] P. Tomei, A simple PD controller for robots with elastic joints, *IEEE Trans. Automat. Control* 36 (10) (1991) 1208–1213, <http://dx.doi.org/10.1109/9.90238>.
- [28] D.J. Inman, *Vibration with Control*, second ed., John Wiley & Sons, 2017.
- [29] H. Troger, A. Steindl, *Nonlinear Stability and Bifurcation Theory an Introduction for Engineers and Applied Scientists*, Springer-Verlag Wien, 1991.
- [30] B. Hazel, J. Côté, Y. Laroche, P. Mongenot, A portable, multiprocess, track-based robot for in situ work on hydropower equipment, *J. Field Robot.* 21 (1) (2012) 69–101, <http://dx.doi.org/10.1002/rob.20425>.
- [31] J. Lessard, G. Swiatek, Z. Liu, B. Hazel, Flexible multibody dynamics and effects of nonlinear joint stiffness for vibration analysis in a robotic grinding process, in: *ECCOMAS-Thematic Conference on Multibody Dynamics*, 2011.
- [32] M.-N. Pham, P. Hamelin, B. Hazel, Z. Liu, A two-stage state feedback controller supported by disturbance-state observer for vibration control of a flexible-joint robot, *Robotica* 38 (6) (2020) 1082–1104, <http://dx.doi.org/10.1017/S0263574719001267>.
- [33] J. Denavit, R. Hartenberg, A kinematic notation for lower-pair mechanisms based on matrices, *J. Appl. Mech.* (1955).
- [34] L.-W. Tsai, *Robot Analysis: The Mechanics of Serial and Parallel Manipulators*, Wiley-Interscience, 2003.
- [35] E. Reynders, J. Houbrechts, G. De Roeck, Fully automated (operational) modal analysis, *Mech. Syst. Signal Process.* 29 (2012) 228–250, <http://dx.doi.org/10.1016/j.ymssp.2012.01.007>.
- [36] V.-H. Vu, M. Thomas, F. Lafleur, L. Marcouiller, Towards an automatic spectral and modal identification from operational modal analysis, *J. Sound Vib.* 332 (1) (2013) 213–227, <http://dx.doi.org/10.1016/j.jsv.2012.08.019>.
- [37] V.-H. Vu, M. Thomas, A. Lakis, L. Marcouiller, Operational modal analysis by updating autoregressive model, *Mech. Syst. Signal Process.* 25 (3) (2011) 1028–1044, <http://dx.doi.org/10.1016/j.ymssp.2010.08.014>.
- [38] T.-T. Do, V.-H. Vu, Z. Liu, NAFID-a grid tool for output only modal analysis, in: *Proceedings SURVISHNO*, 2019, pp. 119–127.